Available online at www.sciencedirect.com

ScienceDirect

journal homepage: www.elsevier.com/locate/issn/15375110

Research Paper

Pore structure of wastewater sludge chars and their water retention impacts in different soils

Mika Turunen [a,*], Jari Hyväluoma [b], Riikka Keskinen [a], Janne Kaseva [a], Johanna Nikama [a], Aino Reunamo [c], Kimmo Rasa [a]

[a] Natural Resources Institute Finland (LUKE), Tietotie 4, 31600, Jokioinen, Finland
[b] Häme University of Applied Sciences, Mustialantie 105, 31310, Mustiala, Finland
[c] BioMediTech, Faculty of Medicine and Health Technology, Tampere University, 33014, Tampere, Finland

ARTICLE INFO

Article history:
Received 17 April 2020
Received in revised form
15 January 2021
Accepted 11 March 2021
Published online 1 April 2021

Keywords:
Interporosity
Intraporosity
Amendment
Pyrolysis
3D imaging
Tomography

Feasibility of pyrolysing wastewater sludge for char and energy production is dependent on the usability of the produced sludge char. This study aimed to produce mechanistic information of char impacts on amended porous media by determining (1) pore structure of sludge chars with 3D image analyses and (2) their influence on water retention and shrinkage properties of three contrasting soils. The pore structure of the chars consisted of crevices and large spheres. Their water retention impacts were minor, even though the low-porous char slightly increased porosity in the amended materials in various pore-size ranges. The dominating, though small, impacts were the increase in easily drainable interpores and decrease in smallest pore sizes relevant for plant available water. The char impacts were more visible in fine-than coarse-textured soils. The chars also significantly reduced shrinkage in clay soils. The results were insensitive to sludge feedstock or char particle size.

1. Introduction

Population growth and technical development of our societies have increased the potential to process and use wastewater resources for various purposes. Additionally, environmental challenges set pressures to find novel and sustainable ways to utilise sewage sludge and preserve its carbon and nutrient content. Pyrolysis of wastewater sludge is one potential approach to manage the waste stream and to produce solid nutrient containing char (hereby referred as sludge char) and gas/liquid fraction for energy production. While there is a range of possibilities to exploit the waste resource (Kroiss, 2004), the thermal processing of the sludge has the benefit that it reduces the waste volume and transport costs (e.g. Méndez, Gómez, Paz-Ferreiro, & Gascó, 2012), produces energy (e.g. Gaunt & Lehmann, 2008), can sequester carbon (e.g. Lehmann, Gaunt, & Rondon, 2006) and reduces pathogens of the substance (e.g. Waqas, Khan, Qing, Reid, & Chao, 2014). The feasibility of the approach is, however, also dependent on the usability of the produced sludge char.

* *Corresponding author*. Natural Resources Institute Finland, Tietotie 4, FI-31600, Jokioinen, Finland.
E-mail addresses: mika.turunen@luke.fi (M. Turunen), jari.hyvaluoma@hamk.fi (J. Hyväluoma), riikka.keskinen@luke.fi (R. Keskinen), janne.kaseva@luke.fi (J. Kaseva), johanna.nikama@luke.fi (J. Nikama), aino.reunamo@tuni.fi (A. Reunamo), kimmo.rasa@luke.fi (K. Rasa).
https://doi.org/10.1016/j.biosystemseng.2021.03.010

One of the most promising applications for the sludge char is to use it for carbon sequestration purposes and as amendment in soils and growing media used in urban landscaping. This approach is comparable to the use of wood-based pyrolysis product called biochar, which has been widely studied compared to the sludge chars. Compared to the wood-based biochars, sludge chars can contain a wide range of potentially harmful substances (Liu et al., 2018; He et al., 2010), which challenges their applicability. Furthermore, knowledge on the benefits of sludge char as a soil amendment is currently incomplete (Liu et al., 2018). One key physical impact of char amendments is their effect on water retention properties of the soil. While many studies have shown the potential benefits of amending soils with wood-based biochar (Edeh, Mašek, & Buss, 2020; Laird, 2008), it is also known that the amendment can have adverse or negligible effects on water retention (e.g. Jeffery et al., 2015; Major, Rondon, Molina, Riha, & Lehmann, 2012). Producing an adequate char for a particular purpose requires a well-designed pyrolysis process (Kinney et al., 2012) and information of relevant physical properties of both the char and the amended material (Rasa et al., 2018; Turunen et al., 2020). Pore structure and surface area are among the most important physical properties controlling hydraulic impacts of biochar (Edeh et al., 2020). However, currently comprehensive knowledge of the pore properties of sludge chars is rare and mechanistic understanding of water retention impacts of the amendment is incomplete.

Several studies have shown that the inherent feedstock material structure largely controls the internal pore structure of the pyrolyzed char (Kameyama, Miyamoto, & Iwata, 2019; Brewer et al., 2014; Turunen et al., 2020). While char internal pores can retain water directly, char amendment can also alter soil structure and porosity by affecting the pore space between the soil and char particles (e.g. Gray, Johnson, Dragila, & Kleber, 2014). While some studies have reported chemical and physical properties of various sludge char materials (Kameyama et al., 2019; Agrafioti, Bouras, Kalderis, & Diamadopoulos, 2013), comprehensive analyses of the pore properties of wastewater sludge char and their impacts on water retention properties of different soils remain limited.

Recent studies (e.g. Rasa et al., 2018; Turunen et al., 2020) have shown how 3D X-ray imaging can produce relatively comprehensive information of biochar pore properties, including pore size distribution, surface areas and structural isotropy of the pores. Such information can be combined with conventional water retention data to mechanically understand how the biochar impacts the retention properties (e.g. Rasa et al., 2018; Turunen et al., 2020). The water retention impacts are often complex and include phenomena and changes related to interporosity (pore space between biochar and soil particles), intraporosity (pores inside biochar particles), soil structure, pore accessibility, water table discontinuity and shrinkage (e.g. Brewer et al., 2014; Gray et al., 2014; Liu, Dugan, Masiello, & Gonnermann, 2017; Turunen et al., 2020). Furthermore, char particle size can have controls on the amendment impacts (de Jesus Duarte, Glaser, & Pellegrino Cerri, 2019; Liu et al., 2017; 2016). Therefore, understanding how different char types impacts in different applications is challenging and in-depth mechanistic understanding of the different factors would be a benefit for the design of char for a particular task.

The objectives of this study were to examine physical properties of sewage sludge char derived from an industrial pilot-scale pyrolysis device and specifically (1) to characterise the pore structure of different sludge chars with 3D imaging and image analyses and (2) to quantify their impacts on water retention and shrinkage properties of three contrasting soils. The objectives were tackled by combining information from the 3D pore structure analyses with more conventional water retention curve measurements. To produce a relatively comprehensive assessment of the topic, the analyses were conducted with three different wastewater sludge chars, three different soils and two different char particle sizes. A mechanistic analysis was considered to be beneficial for estimating whether such char could also be use in other applications relaying on porous materials.

2. Materials and methods

2.1. Sludge chars and soils

Three different sludge chars were produced by pyrolysing sludge from two different wastewater treatment plants (Turku and Espoo, Finland). The three pyrolysis runs were conducted in spring 2019 with electronically heated continuously operated industrial pilot-scale pyrolysis device (Ecomation Ltd., Salo, Finland). The total capacity of the retort is 300–400 kg dry sludge per hour. Prior to pyrolysis, wet sludge (dry matter content around 30%) was dried in a vacuum drier (Ecomation Ltd., Salo, Finland) to dry matter content of 87–94% (Table 1). The different sludges and pyrolysis parameters (Table 1) represented conditions in an industrial pilot-scale device where the feedstock and process parameters are not as consistent as in laboratory scale studies. The temperature and residence time is in a narrow range, but the variability in these factors was assumed to reasonably describe sensitivity of the results to the factors prevailing in practice in large scale biochar production. The sludges used were collected from two largest cities in Finland and thus the produced chars are considered to reasonably represent the type of chars practically available with used technology. The resulting three different char types are hereby called type A, B and C (Table 1). The yield of sludge char varied between 51 and 78% (v/v) of dried material. The pH of the resulting chars was 7.1 (±0.3) and electrical conductivity 2.3 (±1.4) mS cm^{-1}. Density of solids of the chars, determined with the pycnometer, was 2.04 (±0.03) g cm^{-3}. The carbon contents of the chars A, B

Table 1 – Key parameters of the three pyrolysis runs and the resulting char types A-C.

	Run 1 (type A)	Run 2 (type B)	Run 3 (type C)
Sludge origin	Turku	Turku	Espoo
Moisture content prior pyrolysis [w/w]	0.12	0.06	0.13
Pyrolysis T [°C]	450	500	500
Pyrolysis retention time [h]	1	1.5	1.5

and C (determined with dry combustion; CHN628, LECO Corporations, Saint Joseph, USA) were 23, 26 and 24% (w/w), respectively.

The impacts of the produced sludge chars on soil water retention capacity and shrinkage behavior were studied in three contrasting soils representing typical Finnish fine and coarse textured soils: coarse sand soil was collected from eastern Finland (Keskinen, Hyväluoma, Sohlo, Rasa, 2019), fine clay loam topsoil from southwest Finland (e.g. Uusitalo, Lemola, & Turtola, 2018) and commercial artificial organic growing medium comprising of sand, composted sewage sludge and horse manure (hereby called mull soil; HSY, 2020). The key physical and chemical properties of the studied soils are shown in Table 2 and described in more detail in Keskinen et al. (2019), Uusitalo et al. (2018) and HSY (2020). The soils were oven dried (37 °C) and passed through a 5-mm sieve prior to establishing the experimental treatments consisting of 10% (v/v) amendment of the chars in two size fractions: 0.6–2 mm and <5 mm. The two particle size choices represented mid-range particle sizes (0.6–2 mm) and a wide range of particle sizes (<5 mm) (Fig. 1). Char particle size choice can have controls on the char impacts as an amendment (de Jesus Duarte et al., 2019), and it was assumed that the sensitivity of the results to the size classes can be reasonably described with our two contrasting particle class choices.

The water retention measurements were carried out in metal cylinders with the volume of approximately 200 cm^3 (diameter 72 mm, height 48 mm). First, ten replicates of each non-amended soil were packed by pouring, with the aid of a collar, approximately 300 cm^3 of loose soil to a cylinder sealed at the bottom by a filter paper. Then, the soil was compacted with 35 g cm^{-2} weight under vibration generated by dropping a 2.2 kg weight for five times from a 50-mm height at a 100-mm distance from the cylinder. After the compaction, the soil surface was carefully levelled to the rim of the cylinder and the weight of the packed soil was measured. Thereafter, portions of soils amended with sludge char were constructed by thoroughly mixing 20 cm^3 of char (according to the volume weight of the char type and size fraction in question), to an amount of soil equal to the average packed weight of 200 cm^3 to produce an amendment rate of 10% char (v/v). For reference, the amount of amendment would correspond to approximately 100 t ha^{-1} in field experiments. Finally, the amended and non-amended samples (5 replicates of each) were packed into cylinders as described above. After levelling, the amount of remaining excess material (amended soils) was weighed and converted to volume according to the volume weight of the corresponding packed char-soil mix. The 10% (v/v) char amendment increased the final volume on average by 5.6 (±1.4), 6.2 (±1.9) and 7.7 (±2.9) % in the sand, clay and mull soil, respectively. In total, the sample set consisted of 105 samples, and a summary of the set is given in Table 3.

Specific nano-scale surface areas and pore distributions of the chars were determined from adsorption–desorption isotherms. Nitrogen was used as the adsorbate. These determinations were conducted with a Micromeritics ASAP 2020 instrument (Norcross, GA, USA). With the instrument used, pores down to 1.5 nm in diameter could be measured. To clean the sample surfaces and remove any adsorbed gas, portions of each sample (100–200 mg) were degassed at the pressure of 2 mmHg and at a temperature of 413 K for two hours. Adsorption isotherms were obtained by immersing sample tubes in liquid nitrogen with the temperature of −195.8 °C in order to achieve isothermal conditions. Gaseous nitrogen was put to the samples in small portions. Thus, the resulting isotherms were obtained. Specific nano-scale surface areas were calculated from the adsorption isotherms with the Brunauer–Emmett–Teller (BET) method (Brunauer, Emmett, & Teller, 1938). Furthermore, total nano-scale pore volumes were calculated from the adsorption isotherm at a relative pressure (P/P0) of 0.985 (Seaton, Walton, & Quirke, 1989) assuming slit-formed pores (Lastoskie, Gubbins, & Quirke, 1993).

Table 2 – Key properties of the experimental soils.

Soil	Sand	Clay	Mull
Texture (ISO 11277) [%]			
Clay (<0.002 mm)	6	38	5
Silt (0.002–0.02 mm)	5	21	7
Fine sand (0.02–0.2 mm)	56	30	40
Sand (0.2–2 mm)	33	11	48
Total C [%]	4.2	3.6	6.3
Dry bulk density [g cm^{-3}]	1.1	1.0	0.9
Density of solids [g cm^{-3}]	2.6	2.7	2.5
Amended soils			
pH	6.2	6.2	7.7
EC [mS cm^{-1}]	0.8	0.7	2.2

2.2. Water retention and shrinkage measurements

Prior to the moisture retention measurements, the samples were saturated with water in a sandbox apparatus (Eijkelkamp, Giesbeek, The Netherlands) by holding the water level at the middle of the cylinder height for 14 d. Thereafter, soil moisture characteristic curves were determined by weighing the drying samples after equilibration in suction pressures of 0.1, 0.3, 1.0, 3.2, 5.0, 6.3, 7.9, 10, 13, 16, 20, 25, 32, 40, 63, 100, 320, 1600 and 39,000 kPa. The 0.1 and 0.3 kPa equilibration step was conducted in the sand box and steps from 1.0 to 320 kPa on ceramic plates in pressure extractors (Soilmoisture Equipment Corp., Goleta, USA). The highest suction pressures, 1600 and 39,000 kPa, were measured in desiccators by vapour pressure equilibrium with saturated ammonium oxalate and sodium chloride solution, respectively, using unpacked, finely ground (<0.4 mm) samples.

The shrinkage of the samples at each suction pressure step until the vapour pressure equilibrium phase was measured vertically at five locations per sample by a Vernier caliper and horizontally from four locations per sample by a feeler gauge.

2.3. 3D imaging and image analyses

The 3D imaging of the sludge chars was conducted with a Zeiss Xradia MicroXCT-400 (Zeiss, Pleasanton, USA) X-ray microtomography scanner. The projection angle was 360 with 1601 projections and a 20x objective was used with binning 2. The source voltage was 100 kV, source current 100 μA and an exposure time of 10 s was used. This resulted in a voxel size of 1.1 μm. All samples were imaged with same parameter values.

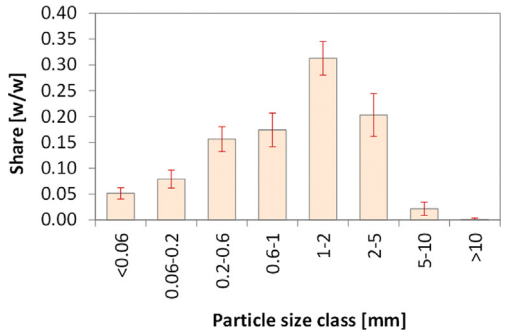

Fig. 1 – Particle size distribution of the sludge char material.

The 3D reconstruction was created of the projections with filtered back projection algorithm using the Zeiss XMReconstructor software (Zeiss, Pleasanton, USA).

The obtained greyscale image stacks were filtered with a 3D variance-weighted mean filter (Gonzales & Woods, 2008; Turpeinen, 2015) with radius 5. The filtered images were segmented into solid and void phases with the segmentation method developed by Hapca, Houston, Otten, and Baveye (2013). This method is a modification of the method of Otsu (1979) with an additional pre-classification step. Here the standard Otsu method was used as the pre-classification step, i.e., the segmentation was performed by two subsequent Otsu segmentations. Pre-classification was necessary as the wastewater sludge samples contained several solid components with significantly different densities (ranging from organic matter to iron). The selected method led to satisfactory segmentation results as judged by visual inspection. A majority filter with radius 2 was applied to the segmented images and finally small isolated solid objects were interpreted as artefacts and removed from the images. The binary images obtained were used in the image analyses except for isotropy analyses (described below) where the denoised greyscale images were used.

Table 3 – A summary of the studied materials (amended and non-amended).

Soil	Char	Char particle size
Sand	Type A	0.6–2 mm
		<5 mm
	Type B	0.6–2 mm
		<5 mm
	Type C	0.6–2 mm
		<5 mm
	No char (control)	–
Clay	Type A	0.6–2 mm
		<5 mm
	Type B	0.6–2 mm
		<5 mm
	Type C	0.6–2 mm
		<5 mm
	No char (control)	–
Mull	Type A	0.6–2 mm
		<5 mm
	Type B	0.6–2 mm
		<5 mm
	Type C	0.6–2 mm
		<5 mm
	No char (control)	–
Total number of materials:		21
Total number of samples:		105

The images were analysed for porosity, pore size distribution, specific surface area, and structural anisotropy (see Hyväluoma et al., 2018 for details). Porosity is the fraction of pore volume in the imaged sample and was obtained as the quotient between the number of pore voxels and the total number of voxels in the image. Pore size distribution was calculated by successive application of a morphological opening operation (Horgan, 1998) with increasing diameter of the structuring element. The specific surface area was defined here as the total surface area per bulk volume and calculated from the number of pore-to-solid transitions, using a method based on Minkowski functionals (Vogel, Weller, & Schlüter, 2010). Structural anisotropy was determined using the greyscale gradient structure tensor and quantified as the degree of anisotropy D_A (Tabor & Rokita, 2007). D_A value close to unity describes an isotropic pore structure and a higher value indicates a stronger structural anisotropy. For sludge char structures with clear anisotropic features, such as the cellular structure of wood-based materials, typically $D_A > 20$, whereas for nearly isotropic materials $D_A < 2$ (see Hyväluoma et al., 2018 for reference values determined for several biochars).

2.4. Soil porosity

Effect of the amendments on the pore size distribution were calculated with the water retention data following Rasa et al. (2018). First, pore diameters corresponding with the suction pressures were estimated with the Laplace–Young equation:

$$d = \frac{4\gamma\cos(\alpha)}{p} \quad (1)$$

where d is the pore diameter [m], γ is the surface tension [N m^{-1}], α the contact angle [°] and p the suction pressure [Pa]. γ was set to 72 mN m^{-1} (e.g. Smith & Gillham, 1999). Assuming perfectly wetting pore walls, α was set to 0. Then, the water contents of the samples were linearly interpolated on 2 μm pore diameter interval. The effect of sludge char was computed as:

$$\Delta V_{[d,d-\Delta d]} = (V_d^{char} - V_{d-\Delta d}^{char}) - (V_d^{no\_char} - V_{d-\Delta d}^{no\_char}) \quad (2)$$

where ΔV [m^3 m^{-3}] is the effect of char amendment on pore volume in each 2 μm pore size interval, V [m^3 m^{-3}] is the volume fraction of soil water in the sample, *char* denotes samples with char and *no_char* denotes samples without char, p is the upper limit and d-Δd lower limit of pore size interval (d = 2.01 μm, d = 4.01 μm, d = 6.01 μm, …; Δd = 2 μm).

2.5. Statistical analyses

The 3D image analysis results (porosities, specific surface areas and degrees of anisotropy) of the A, B, and C type chars were analyzed using the one-way analysis of variance (ANOVA). The assumption of homogeneity of variances was tested and rejected based on a likelihood ratio test, improvement in AICC value or the normality of residuals for every variable. The same model was used to analyze the BET results. However, the nano-scale specific surface areas were analyzed with gamma distribution (with log link) because of heteroscedasticity of residuals.

Moisture data was analyzed separately for each three soil using generalised linear models. The assumption of beta (with logit link) distribution was used having treatment (7 materials) and pressure (19 points), and their interaction as fixed effects. Correlated observations between pressure points were taken into account using the most suitable covariance structure, which was compound symmetry (CS) that assumes a constant covariance between all points. Lowest AICC value was used as the most important criterion for selection of covariance structure, together with the normality of the residuals. Differences of means of all treatments were compared within each soil and pressure point (Gbur et al., 2012).

Simplified model without repeated measures (ANOVA) was used for same treatments (7 for each soil) when drainable water, readily plant available water, plant available water and ratio of sample volume to original sample volume in suction pressures (0.1, 10 and 320 kPa) were studied. The assumption of homogeneity of variances was tested and rejected based on a likelihood ratio test, improvement in AICC value or the normality of residuals for every variable. Differences of means of all treatments were compared within each soil and suction pressure.

All models were fitted by using the residual pseudo likelihood (for beta) or restricted maximum likelihood (for the rest) estimation methods, respectively. The method of Westfall (Westfall, 1997) was used for pairwise comparisons of treatments with a significance level of $\alpha = 0.05$. The degrees of freedom were calculated using the Kenward-Roger method (Kenward & Roger, 2009).

The analyses were performed using the GLIMMIX procedure of the SAS Enterprise Guide 7.15 (SAS Institute Inc., Cary, NC, USA).

3. Results and discussion

3.1. Pore structure of the sludge chars

The 3D imaging results showed that the pore structure of A, B and C type sludge char samples were qualitatively and visually similar (Fig. 2), as described in more detail below. The pore space of almost all of the samples consisted of roughly two different types of pores: (1) crevices and smaller individual pores and (2) large peculiar spherical cavities. The large pores that had almost perfect spherical shape and diameters greater than 100 μm were found inside several samples (Fig. 2). Thus, the pore structure of these chars were clearly different than the pore structure of chars produced from wood feedstocks or broiler manure in previous studies (Kameyama et al., 2019; Keskinen et al., 2019; Rasa et al., 2018; Turunen et al., 2020). The pore space in biochars produced from various wood materials often consists of tubular pores reflecting the tissue structure of the feedstock material (Kameyama et al., 2019; Rasa et al., 2018; Turunen et al., 2020). Contrastingly, the crevices in the sludge chars of the current study were probably due to the material structure, thermal processing and drying. The spherical shapes (Fig. 2) probably formed due to entrapment or formation of gas bubbles in the material during vacuum drying (prior to pyrolysis). Van Kessel and Van Kesteren (2002) suggested that formation of gas in a sludge can push aside the surrounding material and form cracks around the bubbles.

Porosities (mean ± standard deviation) of the A, B, and C chars were 0.19 ± 0.03, 0.16 ± 0.02 and 0.16 ± 0.01, respectively. Specific surface areas were 34 ± 3, 33 ± 4, and 31 ± 6 $mm^2\ mm^{-3}$, and degrees of anisotropy 1.24 ± 0.13, 1.34 ± 0.18, and 1.22 ± 0.02, respectively. Differences in these properties between the different char types were not statistically significant ($p \geq 0.18$). The porosity and specific surface area values obtained for wastewater sludge chars were ca. 2–4

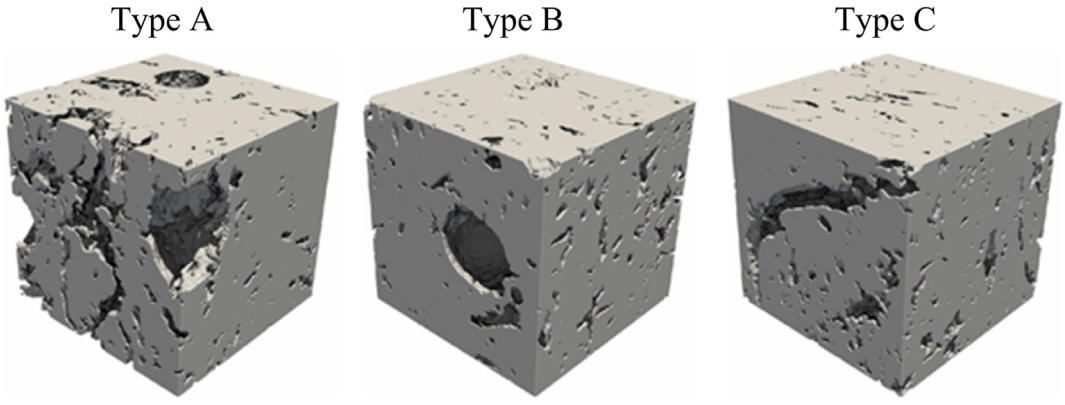

Fig. 2 – X-ray tomographic reconstructions of three imaged sludge char samples of the char types A-C. The size of each visualized subsample is (500 μm)³. The observed spherical pores can be seen on the top edge of the type A sample and on the front-left edge of the type B sample.

times lower than those of wood-based biochars (Hyväluoma et al., 2018) or broiler manure biochars (Keskinen et al., 2019). Porosity and specific surface area are known to be among the key factors determining biochar water retention impacts (Edeh et al., 2020) and thus the low values challenge the usability of the sludge chars. Considering the possibility to modify pore structure of the sludge chars (Fig. 2), it can be hypothesised that an increase of gas bubbles in the feedstock material could increase their porosity. For all samples, the degree of anisotropy was close to unity which indicates that the studied chars were highly isotropic in contrast to, e.g., wood-based biochars (Hyväluoma et al., 2018). Practically, the results reflect the fact that while pores in wood-based biochars are typically tubular and oriented towards a particular direction, the pore structure of the sludge chars did not have a clear orientation towards any direction and can be considered random.

The pore size distributions from the 3D image analyses are shown in Fig. 3. The pore size distributions had longer tails than those of wood-based biochars (Hyväluoma et al., 2018; Turunen et al., 2020). However, the pore sizes were mainly limited below 100 μm and majority of their volume was in pore size regime below 50 μm. Therefore, even though the total pore volume of the present chars was relatively low, the major part of the porosity is able to store water. This is in contrary to the pore space of broiler manure biochar where larger portion of the pore volume comprised of voids that were too large to hold plant available water (Keskinen et al., 2019).

The small but distinct peaks in the tail of the pore size distributions were due to spherical pores within the chars, as exemplified in Fig. 4. Pores with the diameter larger than 100 μm were sphere-shaped (Fig. 2). As an example, Fig. 4a shows the pore size distribution for one A-type sample together with visualization of that part of the pore space which comprised of pores larger than 100 μm (Fig. 4b). Each peak in the distribution in the regime with pore size >100 μm can be attributed to a single spherical pore. While the spherical pores can function as local water or air storages, the pore accessibility is dependent on how they are connected with the surrounding crevices and other pores (Brewer et al., 2014; Liu et al., 2016).

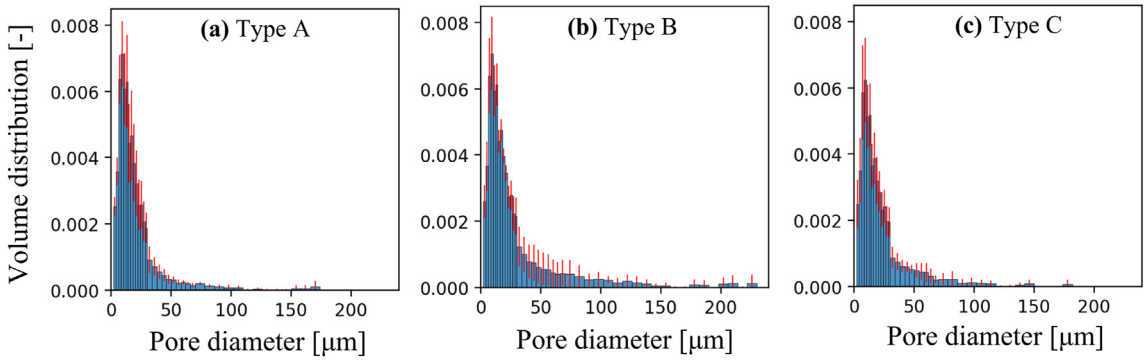

Fig. 3 – Pore size distributions of sludge char types (a) A, (b) B and (c) C. For each char type, the pore size distribution combines mean volume distributions of five replicate samples. Each volume distribution sums to unity. The error bars denote the standard deviation.

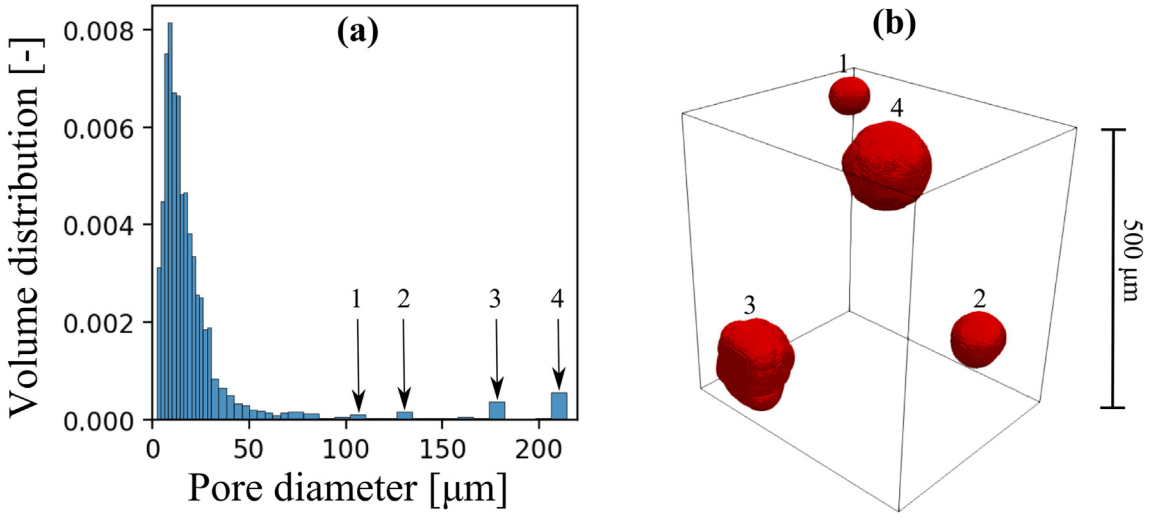

Fig. 4 – (a) Pore size distribution (sums to unity) of a single A-type sludge char sample with four peaks in the pore size range >100 μm (indicated by arrows) and (b) pores with the diameter >100 μm within the char image. The numbers 1–4 show which peak in the distribution in (a) is attributed to which pore in (b).

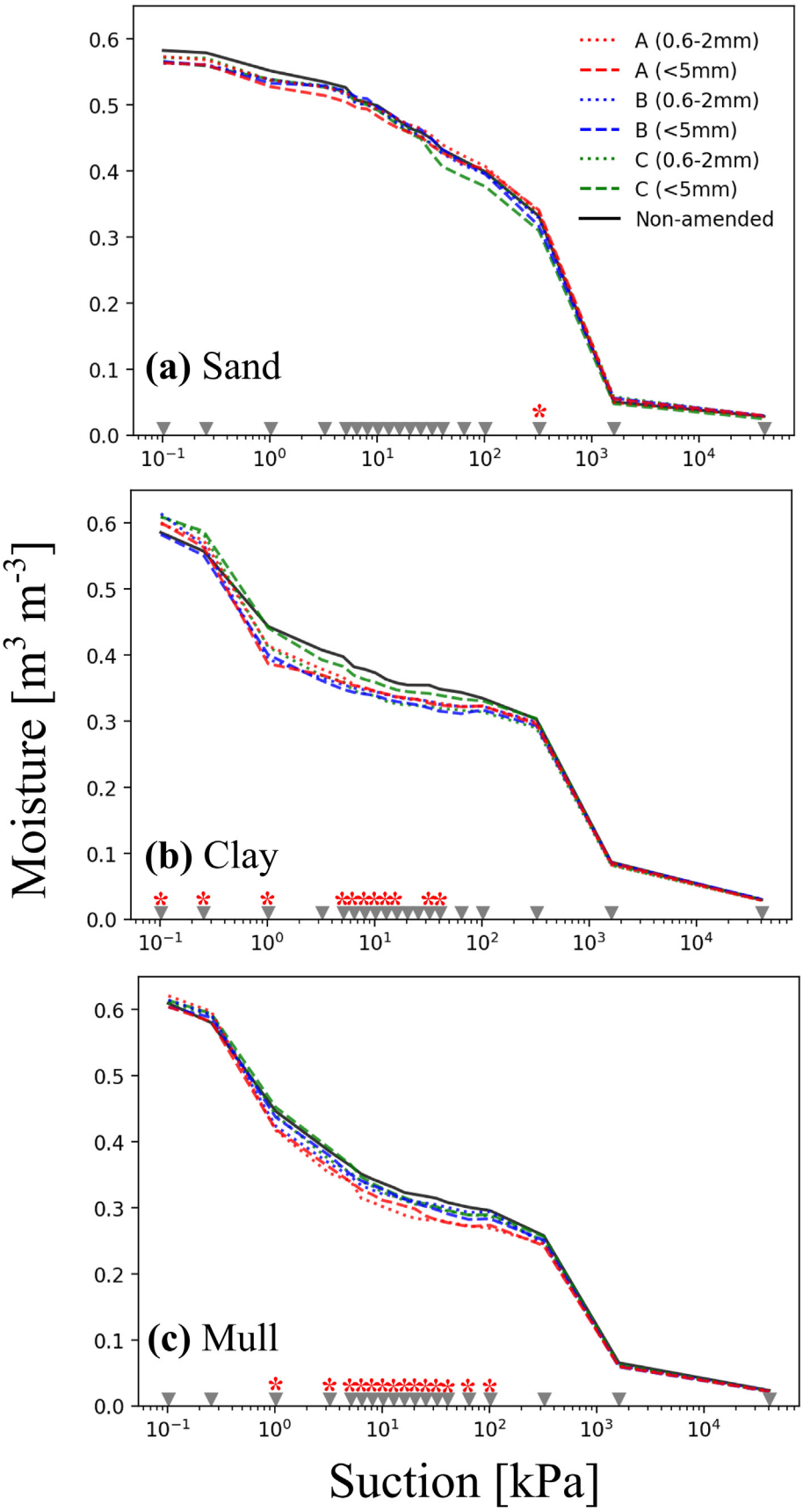

Fig. 5 – Water retention curves of the studied (a) sand, (b) clay and (c) mull soil with and without the three different sludge chars (A–C) and the two different char particle sizes (0.6–2 mm and <5 mm). The triangles denote the suction measurement steps and the asterisks denote those steps where statistical differences between the treatments were detected.

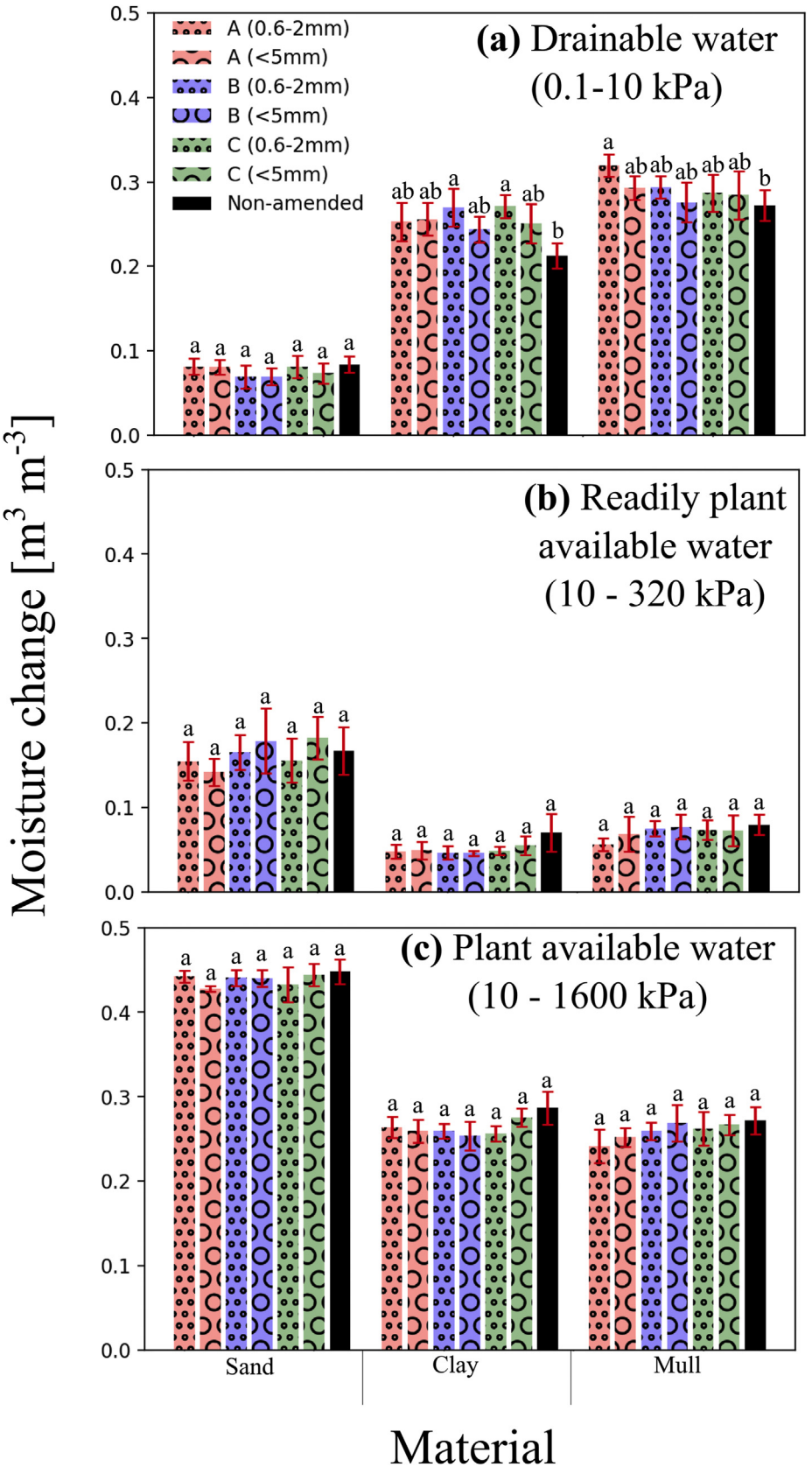

Fig. 6 – (a) Drainable water, (b) readily plant available water and (c) plant available water in the studied sand, clay and mull soils with and without the three different sludge chars (A–C) and the two different char particle sizes (0.6–2 mm and <5 mm). The error bars denote the standard deviation. The different letters (a, b and c) adjacent to the bars denote statistical difference between the materials in a suction pressure within each soil.

It is also noteworthy, that when the pore structure of porous materials is quantified with 3D imaging and image analysis, the obtained results are dependent on the imaging resolution (i.e. voxel size). The binary representation of the solid/void regions describes each voxel as either solid or void. Therefore pores smaller than the imaging resolution are not detected and distinguished. In the present work, the imaging resolution was 1.1 μm and thus comparable to those in our previous studies (Hyväluoma et al., 2018; Keskinen et al., 2019).

Regarding nano-scale pores as probed by gas adsorption measurements, the BET analysis showed specific nano-scale surface areas values of 6.3 (±1.1), 8.4 (±1.7) and 5.8 (±1.2) m^2 g^{-1} in type A, B and C chars, respectively, and there were no statistically significant differences between the char types ($p \geq 0.06$). The specific nano-scale surface areas values were lower than those measured by Zielińska, Oleszczuk, Charmas, Skubiszewska-Zięba, and Pasieczna-Patkowska (2015) (9–54 m^2 g^{-1}) in wastewater sludge chars in Poland and those measured by Gray et al. (2014) (153–280 m^2 g^{-1}) in wood-based biochars, but on the other hand higher than those measured by Turunen et al. (2020) (<1.2 m^2 g^{-1}) in different plant-based biochars. The gas adsorption observations showed nano-scale pore volumes of 0.04 (±0.005), 0.04 (±0.003) and 0.03 (±0.001) cm^3 g^{-1} in A, B and C chars, respectively. The pore volumes of type B char differed from those of the types A and C ($p \leq 0.03$), which demonstrates that sludge char feedstock and pyrolysis can have an impact on nano-scale pores. The values were comparable to the range of 0.03–0.09 cm^3 g^{-1} measured by Zielińska et al. (2015). Based on our pycnometer and pore volume measurements we further calculated the nano-scale porosity of 0.08 (±0.009), 0.09 (±0.006) and 0.06 (±0.002) in type A, B and C chars, respectively. Comparison of the 3D imaging results and the nano-scale porosities points out that a clear majority of the porosity in the chars resided in pores larger than 1 μm, but also the role of nano-scale porosity was substantial. For comparison, Turunen et al. (2020) found negligible nano-scale porosities in different biochars. Our analyses further showed that clear majority (76 ± 0.01%) of the nano-scale pore volume resided in mesopores (2–50 nm), while macropores (>50 nm) comprised a minor share (24 ± 0.01%) of the volume and the share of smaller pores (<2 nm) was negligible. In plant-based chars, nano-scale pores are typically pyrogenic (Fu et al., 2012; Gray et al., 2014) and it may be hypothesised that they were formed due to the pyrolysis also in the studied sludge chars.

3.2. *Water retention and shrinkage impacts*

The water retention curves of the sandy soil were clearly different to the curves of the clay and mull soils (Fig. 5). The clay and mull soils released a large share of moisture in the suction range <10 kPa, while the sand soil retained more water in that pressure range. Practically, char amendments did not affect the water retention properties of the sandy soil. However, statistical differences ($p < 0.05$) between the studied materials in the different soils were found especially in the clay and mull materials (Fig. 5), which demonstrates that the amendments had small but significant impacts on their water retention properties. Note also that the differences between the studied soils were higher than the differences between the amended and non-amended materials (Fig. 5).

In the clay and mull soils 3 out of 12 char treatments increased the amount of drainable water ($p < 0.05$; Fig. 6a) and the impact was the clearest in the clay soil. This was attributed to the interporosity impact, since the impact was similar also in such suction pressures ranges where only a minor share of the char pores prevailed. Interporosity impacts due to various biochar amendments have been noted also previously (e.g. Gray et al., 2014; Liu et al., 2016; Liu et al., 2017), but these and other impacts of sludge char have been rarely quantitatively assessed. On the other hand, the increase of drainable water due to the sludge char additions could be partly attributed to impacts of the amendment on the clay soil structure (Sun & Lu, 2014). In either case, practical implications of the char amendments were minor. Knowledge on the benefits of sludge char as a soil amendment is scarce (Liu et al., 2018). However, previously also Sun and Lu (2014) found sludge char to impact drainable water in a clayey soil and found no impacts on other common water retention parameters. Our study approach which combined detailed information on the pore properties of sludge chars provided a mechanistic explanation on how the water retention properties can be impacted by the amendments.

Practically minor water retention impacts of the chars were further highlighted by the fact that amendment impacts on readily plant available water and plant available water were not statistically significant in any of the materials ($p \geq 0.09$; Fig. 6b-c). It is also noteworthy that the differences between the impacts of the different chars (varying sludge feedstock, pyrolysis parameters and particle size) were typically not statistically significant (Fig. 6). I.e., the impacts of the char amendments on the water retention properties of the different soils were not sensitive to the char pyrolysis process, feedstock and particle size. This implies that, in terms of water retention, rather homogeneous sludge chars can be produced with the industrial pilot-scale device and varying feedstock properties.

While the practical impacts of the char amendments regarding their usability are described by the variables in Fig. 6, our methodological approach also demonstrated a more in-depth assessment on how sludge char can mechanistically impact water retention of the studied materials (Fig. 7). The clearest impact of the char amendment (when analyzed in the 2 μm pore diameter intervals) was that it typically decreased the amount of small pores (≤6 μm diameter) in the soil samples. The effect was likely due to replacement of such soil material which contained small pore sizes with the char particles which contained lower amount of small pores. The char amendments did typically slightly increase porosity in a few pore size ranges shown in Fig. 7. However, the increases were small compared to the impacts of willow biochar observed in a previous study (Rasa et al., 2018).

In near-saturated conditions (0.1 kPa) the samples typically swelled, and the swelling was the highest in the mull samples (Fig. 8). The samples shrunk with desorption. Clear differences ($p \leq 0.04$) between the amended and non-amended materials were found only in the clay samples in 320 kPa, where the non-amended material differed from all of the amended materials. Thus, in addition to the water retention impacts, the sludge

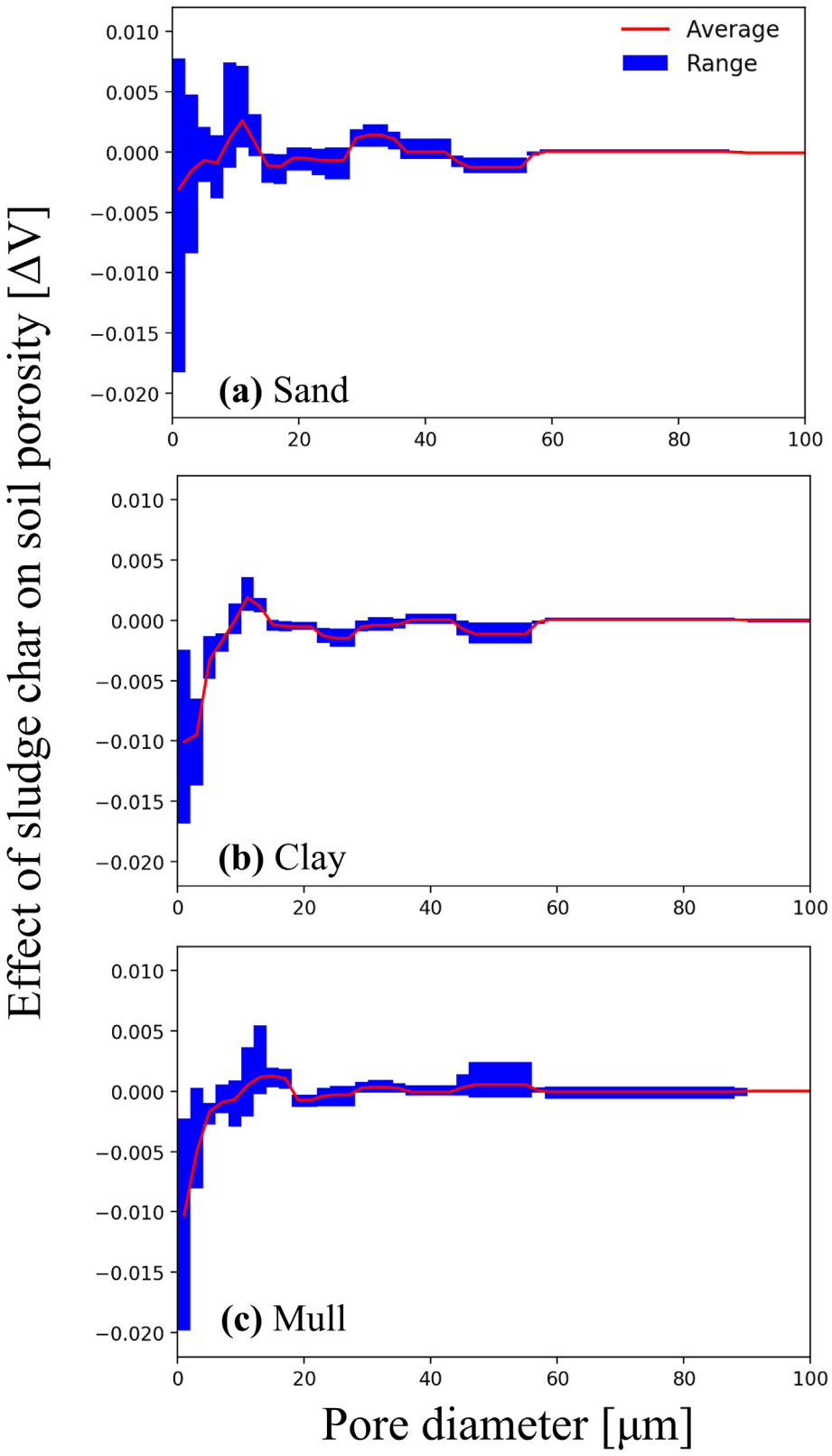

Fig. 7 – Effect of sludge char on soil porosity in the studied (a) sand, (b) clay and (c) mull soils. The blue bars denote the range of the mean effects of the different cases (three different sludge chars and two different char particle sizes). The red line denotes the average impact. The effect was calculated using Eq. (2) and thus a positive value denotes that the porosity is higher in an amended sample than in a non-amended sample (in a 2 μm interval). (For interpretation of the references to colour in this figure legend, the reader is referred to the Web version of this article.)

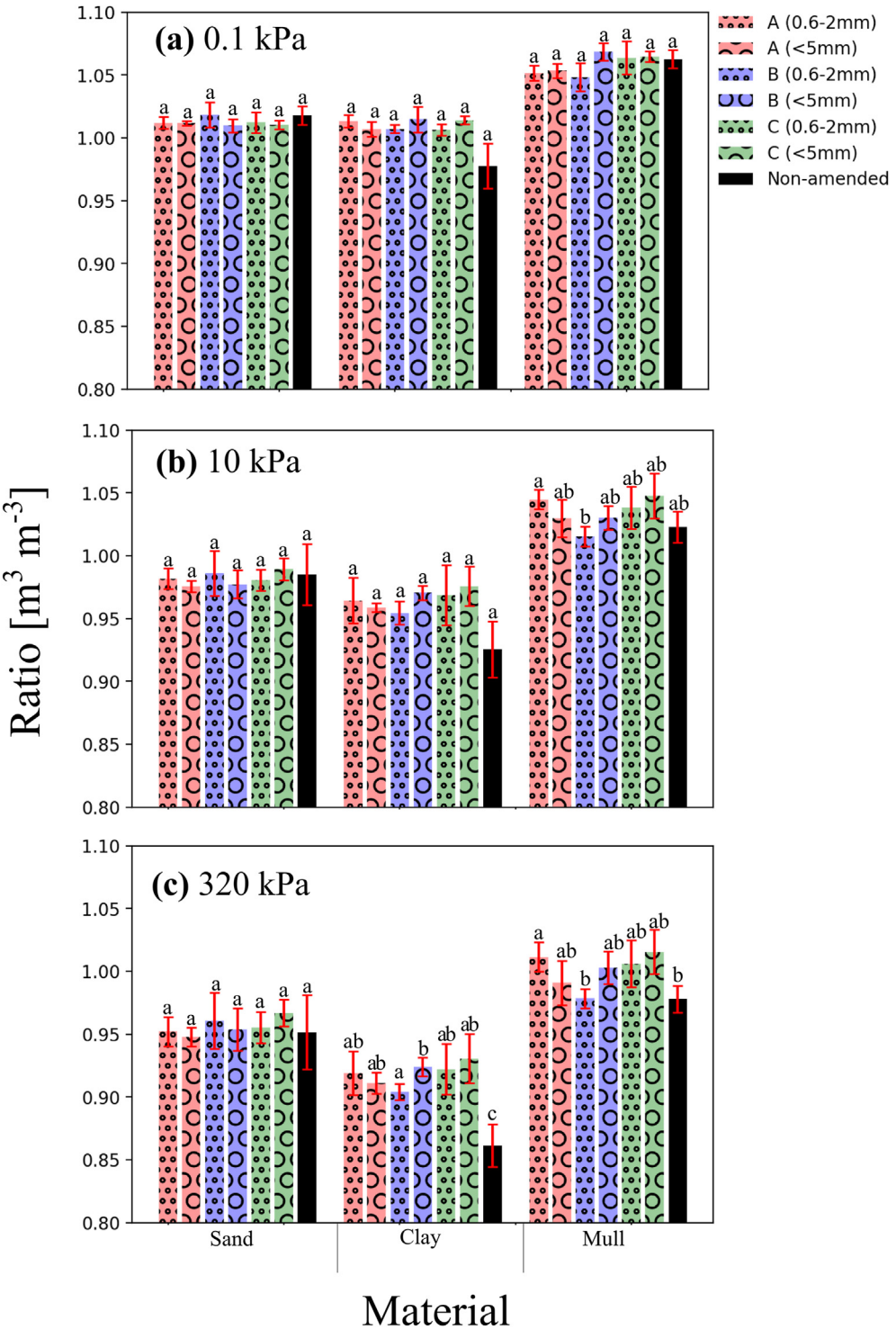

Fig. 8 – Ratio of sample volume to original sample volume in suction pressures (a) 0.1 kPa, (b) 10 kPa and (c) 320 kPa in the studied soils with and without the three different sludge chars (A–C) and the two different char particle sizes (0.6–2 mm and <5 mm). The error bars denote the standard deviation. The different letters (a, b and c) adjacent to the bars denote statistical difference between the materials in a suction pressure within each soil.

chars can have clear impacts on shrinkage in clay soils. Since the amended clay soil samples shrunk less than the non-amended samples, the char impact on drainable water (Fig. 6) was probably not due to increases in shrinkage cracks, but can be attributed to increases in interparticle porosity. Regarding shrinkage, Turunen et al. (2020) found no marked differences in the shrinkage of moss growing media with and without biochar amendments, but suggested that char particle size might have an impact on the amount of shrinkage. The results of the current study with the two different sludge char particle sizes

showed no systematic differences between two different char particle size distributions, even though the particle size caused differences in the shrinkage of clay in 320 kPa (Fig. 8). The chars A-C also had different impacts on the shrinkage of the clay and mull soils. This implies that variability in process and sludge parameters can cause small but statistically significant differences in the shrinkage behavior of amended soils.

Overall, based on the results, the minor effect of sludge char on soil water retention is a combination of several different mechanisms altering pore size distribution of the amended material. Both the interporosity impact and the impact of replacing relatively porous soil material with low-porous char were higher than the small impact of intra-porosity. In applications in fine-textured soils, increase in large and easily drained interpores may diminish the water retention impact of the char intrapores. The impact of char amendment is known to depend on the amended soil and often the impact is expected to be higher in coarse-than fine-textured soils (e.g. Edeh et al., 2020; Razzaghi, Obour, & Arthur, 2020; Mukherjee & Lal, 2013). Our results show that the water retention impact of sludge char can be higher in fine-textured soils. Wood-based biochars with relatively high porosity add porosity to such pore size ranges where coarse-textured soils have low pore volume. With respect to sludge chars, this mechanism is less important due to lower porosity of the char. On the other hand, interpore effect is clearer in structured fine-textured soils and affects less in non-structural coarse-textured soil, as shown by the water retention curves (Fig. 5). The different pore properties of wood-based biochars and sludge chars can thus lead to contrasting influence in fine- and coarse-textured soils. Previous studies (Edeh et al., 2020) have shown that laboratory scale studies often yield to different results than field-scale studies. However, the mechanisms occurring in sample scale have the potential to explain the key physical phenomena occurring in field scale. Overall, despite the several above-described mechanisms, the practical implications of the sludge char addition on the water retention properties of the soils were minor. Methods to increase porosity in sludge chars would be worth studying to improve their usability. Despite the minor water retention impacts, previous studies have demonstrated that the carbon sequestration potential of sludge chars can be considered to be an environmental benefit, even though the carbon content of the chars is typically smaller than that of biochars (Liu et al., 2018). Also our sludge char carbon content measurements showed that the sludge chars produced in the pilot scale conditions can contain 23–26% (w/w) of carbon.

4. Conclusions

Pore structure of sludge chars consisted mainly of crevices and large spheres. Water retention impacts of the char amendments were minor, but the low-porous char slightly increased porosity in the amended materials in various pore-size ranges. However, the dominating impacts were the increase in easily drainable interpores and decrease in smallest pore sizes relevant for plant available water. Contrasting previous studies with wood-based biochars, the char impacts were more visible in fine-than coarse-textured soils. Reduction in the shrinkage of clay soils was an important secondary amendment impact. The results were insensitive to sludge feedstock or char particle size.

Declaration of competing interest

The authors declare that they have no known competing financial interests or personal relationships that could have appeared to influence the work reported in this paper.

Acknowledgements

We acknowledge the Ministry of the Environment of Finland for financial support in the experimental phase.

REFERENCES

Agrafioti, E., Bouras, G., Kalderis, D., & Diamadopoulos, E. (2013). Biochar production by sewage sludge pyrolysis. *Journal of Analytical and Applied Pyrolysis, 101*, 72–78.

Brewer, C. E., Chuang, V. J., Masiello, C. A., Gonnermann, H., Gao, X., Dugan, B., et al. (2014). New approaches to measuring biochar density and porosity. *Biomass and Bioenergy, 66*, 176–185.

Brunauer, S., Emmett, P. H., & Teller, E. (1938). Adsorption of gases in multimolecular layers. *Journal of the American Chemical Society, 60*, 309–319. https://doi.org/10.1021/ja01269a023

de Jesus Duarte, S., Glaser, B., & Pellegrino Cerri, C. E. (2019). Effect of biochar particle size on physical, hydrological and chemical properties of loamy and sandy tropical soils. *Agronomy, 9*, 165.

Edeh, I. G., Mašek, O., & Buss, W. (2020). A meta-analysis on biochar's effects on soil water properties–New insights and future research challenges. *The Science of the Total Environment*, 136857.

Fu, P., Hu, S., Xiang, J., Sun, L., Su, S., & Wang, J. (2012). Evaluation of the porous structure development of chars from pyrolysis of rice straw: Effects of pyrolysis temperature and heating rate. *Journal of Analytical and Applied Pyrolysis, 98*, 177–183.

Gaunt, J. L., & Lehmann, J. (2008). Energy balance and emissions associated with biochar sequestration and pyrolysis bioenergy production. *Environmental Science & Technology, 42*, 4152–4158.

Gbur, E. E., Stroup, W. W., McCarter, K. S., Durham, S., Young, L. J., Christman, M., et al. (2012). *Analysis of generalized linear mixed models in the agricultural and natural resources sciences*. Madison, WI: American Society of Agronomy, 2012.

Gonzales, R. Z., & Woods, R. E. (2008). *Digital image processing* (3rd ed.). Upper Saddle River: Prentice Hall.

Gray, M., Johnson, M. G., Dragila, M. I., & Kleber, M. (2014). Water uptake in biochars: The roles of porosity and hydrophobicity. *Biomass and Bioenergy, 61*, 196–205.

Hapca, S. M., Houston, A. N., Otten, W., & Baveye, P. C. (2013). New local thresholding method for soil images by minimizing grayscale intra-class variance. *Vadose Zone Journal, 12*. vzj2012.0172.

He, Y. D., Zhai, Y. B., Li, C. T., Yang, F., Chen, L., Fan, X. P., et al. (2010). The fate of Cu, Zn, Pb and Cd during the pyrolysis of

sewage sludge at different temperatures. *Environmental Technology, 31*, 567–574.
Horgan, G. (1998). Mathematical morphology for analysing soil structure from images. *European Journal of Soil Science, 49*, 161–173.
HSY. (2020). *Tuoteseloste – metsäpirtin biomulta*. Available at: https://metsapirtinmulta.fi/wp-content/uploads/2019/03/metsapirtin_biomulta.pdf. (Accessed 17 December 2020).
Hyväluoma, J., Kulju, S., Hannula, M., Wikberg, H., Källi, A., & Rasa, K. (2018). Quantitative characterization of pore structure of several biochars with 3D imaging. *Environmental Science and Pollution Research, 25*, 25648–25658.
Jeffery, S., Meinders, M. B., Stoof, C. R., Bezemer, T. M., van de Voorde, T. F., Mommer, L., et al. (2015). Biochar application does not improve the soil hydrological function of a sandy soil. *Geoderma, 251*, 47–54.
Kameyama, K., Miyamoto, T., & Iwata, Y. (2019). The preliminary study of water-retention related properties of biochar produced from various feedstock at different pyrolysis temperatures. *Materials, 12*, 1732.
Kenward, M. G., & Roger, J. H. (2009). An improved approximation to the precision of fixed effects from restricted maximum likelihood. *Computational Statistics & Data Analysis, 53*, 2583–2595.
Keskinen, R., Hyväluoma, J., Sohlo, L., & Rasa, K. (2019). Fertilizer and soil conditioner value of broiler manure biochars. *Biochar, 1*, 259–270.
Kinney, T. J., Masiello, C. A., Dugan, B., Hockaday, W. C., Dean, M. R., Zygourakis, K., et al. (2012). Hydrologic properties of biochars produced at different temperatures. *Biomass and Bioenergy, 41*, 34–43.
Kroiss, H. (2004). What is the potential for utilizing the resources in sludge? *Water Science and Technology, 49*, 1–10.
Laird, D. A. (2008). The charcoal vision: A win–win–win scenario for simultaneously producing bioenergy, permanently sequestering carbon, while improving soil and water quality. *Agronomy Journal, 100*, 178–181.
Lastoskie, C., Gubbins, K. E., & Quirke, N. (1993). Pore size heterogeneity and the carbon slit pore: A density functional theory model. *Langmuir, 9*, 2693. https://doi.org/10.1021/la00034a032
Lehmann, J., Gaunt, J., & Rondon, M. (2006). Bio-char sequestration in terrestrial ecosystems–a review. *Mitigation and Adaptation Strategies for Global Change, 11*, 403–427.
Liu, Z., Dugan, B., Masiello, C. A., Barnes, R. T., Gallagher, M. E., & Gonnermann, H. (2016). Impacts of biochar concentration and particle size on hydraulic conductivity and DOC leaching of biochar–sand mixtures. *Journal of Hydrology, 533*, 461–472.
Liu, Z., Dugan, B., Masiello, C. A., & Gonnermann, H. M. (2017). Biochar particle size, shape, and porosity act together to influence soil water properties. *PloS One, 12*, Article e0179079.
Liu, Z., Singer, S., Tong, Y., Kimbell, L., Anderson, E., Hughes, M., et al. (2018). Characteristics and applications of biochars derived from wastewater solids. *Renewable and Sustainable Energy Reviews, 90*, 650–664.
Major, J., Rondon, M., Molina, D., Riha, S. J., & Lehmann, J. (2012). Nutrient leaching in a Colombian savanna Oxisol amended with biochar. *Journal of Environmental Quality, 41*, 1076–1086.
Méndez, A., Gómez, A., Paz-Ferreiro, J., & Gascó, G. (2012). Effects of sewage sludge biochar on plant metal availability after application to a Mediterranean soil. *Chemosphere, 89*, 1354–1359.
Mukherjee, A., & Lal, R. (2013). Biochar impacts on soil physical properties and greenhouse gas emissions. *Agronomy, 3*, 313–339.
Otsu, N. (1979). A threshold selection method from gray-level histograms. *IEEE Transactions on Systems, Man, and Cybernetics, 9*, 62–66.
Rasa, K., Heikkinen, J., Hannula, M., Arstila, K., Kulju, S., & Hyväluoma, J. (2018). How and why does willow biochar increase a clay soil water retention capacity? *Biomass and Bioenergy, 119*, 346–353.
Razzaghi, F., Obour, P. B., & Arthur, E. (2020). *Does biochar improve soil water retention? A systematic review and meta-analysis. Geoderma*, Article 114055.
Seaton, N. A., Walton, J. P. R. B., & Quirke, N. (1989). A new analysis method for the determination of the pore size distribution of porous carbons from nitrogen adsorption measurements. *Carbon, 27*, 853–861. https://doi.org/10.1016/0008-6223(89)90035-3
Smith, J. E., & Gillham, R. W. (1999). Effects of solute concentration–dependent surface tension on unsaturated flow: Laboratory sand column experiments. *Water Resources Research, 35*, 973–982.
Sun, F., & Lu, S. (2014). Biochars improve aggregate stability, water retention, and pore-space properties of clayey soil. *Journal of Plant Nutrition and Soil Science, 177*, 26–33.
Tabor, Z., & Rokita, E. (2007). Quantifying anisotropy of trabecular bone from gray-level images. *Bone, 40*, 966–972.
Turpeinen, T. (2015). *Analysis of microtomographic images of porous heterogeneous materials*. PhD thesis. University of Jyväskylä. Jyväskylä Studies in Computing.
Turunen, M., Hyväluoma, J., Heikkinen, J., Keskinen, R., Kaseva, J., Hannula, M., et al. (2020). Quantifying the pore structure of different biochars and their impacts on the water retention properties of Sphagnum moss growing media. *Biosystems Engineering, 191*, 96–106.
Uusitalo, R., Lemola, R., & Turtola, E. (2018). Surface and subsurface phosphorus discharge from a clay soil in a nine-year study comparing no-till and plowing. *Journal of Environmental Quality, 47*, 1478–1486.
Van Kessel, T., & Van Kesteren, W. G. M. (2002). Gas production and transport in artificial sludge depots. *Waste Management, 22*, 19–28.
Vogel, H. J., Weller, U., & Schlüter, S. (2010). Quantification of soil structure based on Minkowski functions. *Computers & Geosciences, 36*, 1236–1245.
Waqas, M., Khan, S., Qing, H., Reid, B. J., & Chao, C. (2014). The effects of sewage sludge and sewage sludge biochar on PAHs and potentially toxic element bioaccumulation in Cucumis sativa L. *Chemosphere, 105*, 53–61.
Westfall, P. H. (1997). Multiple testing of general contrasts using logical constraints and correlations. *Journal of the American Statistical Association, 92*, 299–306.
Zielińska, A., Oleszczuk, P., Charmas, B., Skubiszewska-Zięba, J., & Pasieczna-Patkowska, S. (2015). Effect of sewage sludge properties on the biochar characteristic. *Journal of Analytical and Applied Pyrolysis, 112*, 201–213.